Thermally tunable lithium-niobate long-period waveguide grating filter fabricated by reactive ion etching

Jin, Wei; Chiang, Kin Seng; Liu, Qing

Published in:
Optics Letters

Published: 15/02/2010

Document Version:
Post-print, also known as Accepted Author Manuscript, Peer-reviewed or Author Final version

Publication record in CityU Scholars:
Go to record

Published version (DOI):
10.1364/OL.35.000484

Publication details:
Jin, W., Chiang, K. S., & Liu, Q. (2010). Thermally tunable lithium-niobate long-period waveguide grating filter fabricated by reactive ion etching. *Optics Letters*, *35*(4), 484-486. https://doi.org/10.1364/OL.35.000484

Thermally tunable lithium-niobate long-period waveguide grating filter fabricated by reactive ion etching

Wei Jin, Kin Seng Chiang,* and Qing Liu

Department of Electronic Engineering, City University of Hong Kong, 83 Tat Chee Avenue, Kowloon, Hong Kong, China

Corresponding author: eeksc@cityu.edu.hk

We fabricate a long-period grating band-rejection filter with a lithium niobate ($LiNbO_3$) channel waveguide, where the grating is formed on the waveguide surface by plasma reactive ion etching. The filter shows three distinct thermal tuning regimes. Below ~55 °C, the center wavelength of the rejection band decreases linearly with an increase in the temperature at a high sensitivity (–1.4 nm/°C). The temperature sensitivity drops abruptly to a negligible value at ~55 °C and stays low up to ~70 °C, above which it jumps abruptly to a large positive value (1.6 nm/°C). We attribute these peculiar tuning characteristics to the formation of different crystal phases in the core and cladding areas of the $LiNbO_3$ waveguide and the abrupt transitions of the thermo-optic coefficients of some crystal phases. The grating could be developed into various kinds of integrated-optic filters and switches for application in optical signal processing.

OCIS codes: 050.2770, 130.3730, 130.7408, 230.7370, 230.7408.

Lithium niobate ($LiNbO_3$) is a mature material for the realization of active optical devices, thanks to its excellent electro-optic, acousto-optic, photorefractive, and nonlinear properties [1]. Grating structures in $LiNbO_3$ waveguides, in particular, form the basis of many integrated-optic components for application in optical sensing and communications. Over the years, a number of techniques have been demonstrated for the fabrication of $LiNbO_3$ waveguide Bragg gratings for narrow-band applications, which include, for example, surface corrugation [2,3], photorefractive recording [3], and periodic proton-exchange [4]. Recently, the structure of long-period waveguide grating (LPWG) has been proposed for the realization of broadband filters [5-7]. The grating is designed to couple light from the guided core mode to a co-propagating cladding mode and has a typical pitch of 10 – 100 μm. LPWGs have negligible reflection and are easier to fabricate than Bragg gratings because of their much longer pitches. To form an LPWG in a $LiNbO_3$ waveguide, however, it is necessary to create a cladding in the waveguide to support one or more cladding modes. We have fabricated such a clad waveguide structure in $LiNbO_3$ with a two-step proton-exchange (PE) technique [8] and subsequently demonstrated an electro-optic LPWG-based filter [9]. In this paper, we present a <u>robust single-material thermally tunable</u> LPWG filter, where the grating is produced along a clad $LiNbO_3$ channel waveguide by plasma reactive ion etching (RIE). We find that the temperature sensitivity of the resonance wavelength of the grating has a large negative value below ~55 °C, but it drops abruptly to a negligible value at ~55 °C and remains low up to ~70 °C, above which it jumps abruptly to a large positive value. This strange U-shaped thermal tuning curve is a new finding that cannot be predicted from our previous studies [8,9], where the gratings were tested at relatively low temperatures. As to be shown, our analysis of this property of the grating sheds new light on the understanding of the phase transitions in PE $LiNbO_3$ waveguides. From a practical point of view, the grating offers a wide wavelength-tuning range and has the potential to be further developed into new $LiNbO_3$-based devices for application in optical signal processing.

Figure 1 shows a schematic diagram of the LPWG filter, where a corrugation grating is formed on the surface of a $LiNbO_3$ waveguide that consists of a core embedded in a slab cladding. To fabricate the device, we started with a polished z-cut, y-propagation $LiNbO_3$ substrate with a dimension of 10 × 22 × 0.5 mm (width × length × thickness) and employed a two-step PE process [8] to form a clad $LiNbO_3$ channel waveguide. We first submerged the substrate into stearic acid at 250 ^oC for 4 hours and then annealed it at 400 ^oC for 70 minutes, which resulted in a PE slab waveguide. Using a prism-coupler system (Metricon, Model 2010), we found that the waveguide supported 7 transverse-magnetic (TM) modes at the wavelength 633 nm. From the measured effective indexes, we determined the refractive-index profile of the waveguide with the inverse WKB method [10] and found that the depth of the waveguide was ~3 μm. We next deposited a 200-nm-thick aluminum mask on the surface of the slab waveguide with a thermal evaporation system (Edwards, Model Auto 306). The mask contained a set of 4-μm-wide channels separated by 60 μm. We then submerged the sample into stearic acid at 250 ^oC for 55 minutes. This second PE process resulted in an array of cores formed in the slab cladding. We finally removed the aluminum mask and measured the effective indexes of the channel waveguides with the same prism-coupler system [11].

The channel waveguide supported only one core mode and one cladding mode at the wavelength 1536 nm, whose effective indexes were 2.1782 and 2.1483, respectively. The grating pitch required for coupling between these two modes is $\Lambda = \lambda_0/(N_{co} - N_{cl})$, where N_{co} and N_{cl} are the effective indexes of the core mode and the cladding mode at the resonance wavelength λ_0 [5]. We chose a grating pitch of 54 μm, which should produce a rejection band at ~1600 nm at the room temperature. We next spin-coated a photoresist film with a thickness of ~1 μm on the sample and formed a grating mask by photolithography. We then etched the masked sample with an RIE machine (Plasma-Therm, Model 790 Series), where the gas used was CF4 (at a flow rate of 3.0 cm^3/min) and the discharge pressure and power were set at 75 mTorr and 100 W, respectively. The corrugation grating had a length of ~16 mm and a width of ~1 mm, which was sufficient to cover a large number of waveguides. Figure 2(a) is an optical image of the grating structure, where the locations of the waveguides are also highlighted. We measured the grating profile with a step profiler (Ambios Technology, Model XP-2). The etching depth of the grating was only ~10 nm, as shown in Fig 2(b), which should be small enough not to cause any significant scattering loss. The propagation loss of the guided core mode of the LPWG was ~0.7 dB/cm at 1550 nm, measured at the room temperature. As shown in Fig. 2, the grating has good uniformity. We could control the etching rate and hence the etching depth by adjusting the discharge pressure or power. In our experiments, the etching time was 2.0 minutes, so the etching rate was 5.0 nm/min. As shown by our results, RIE is a highly effective technique for the writing of long-period gratings on $LiNbO_3$. In fact, RIE has been employed for the fabrication of sophisticated waveguide structures in $LiNbO_3$, which required much deeper etching [12,13].

We measured the transmission spectrum of the grating with a broadband light source and an optical spectrum analyzer and placed a heat pump under the waveguide to control its operating temperature. We observed a rejection band at 1584 nm with a contrast of 12 dB at 25 °C. To demonstrate the operation principle of the grating, Fig. 3(a) and (b) show the near-field images of the output light taken by an infrared vidicon camera (Hamamatsu, Model C2741-03) at the resonance wavelength 1584 nm and an off-resonance wavelength 1560 nm, respectively. As shown in Fig. 3, light is coupled from the core mode into the cladding mode at the resonance wavelength, while remains in the core mode at the off-resonance wavelength, as expected.

We next measured the temperature dependence of the transmission spectrum of the grating. Figure 4(a) shows the change of the resonance wavelength with the temperature over the temperature range from 25 to 80 °C. The curve shows a strange U-shape. Below ~55 °C, the resonance wavelength decreases linearly with an increase in the temperature with a sensitivity of −1.4 nm/°C. The resonance wavelength remains almost unchanged from ~55 to ~70 °C and then increases linearly with the temperature with a sensitivity of 1.6 nm/°C. The normalized transmission spectra measured in the temperature ranges 25 – 55.2 °C, 55.2 – 69.5 °C, and 69.5 – 79.5 °C are shown in Fig. 4(b), (c), and (d), respectively. Regardless of the presence of the transition temperature at ~55 °C, we can tune the resonance wavelength over a range of ~40 nm with a temperature control of only ~30 °C (e.g., from 25 – 55 °C). The grating thus functions as an effective wavelength-tunable filter. We should note that the strength of the rejection band varies with the temperature, because the refractive indexes in the waveguide, and hence the mode-field distributions and the coupling efficiency, depend on the temperature. As shown in Fig. 4, the contrast of the grating can reach ~15 dB at certain temperatures and the bandwidth is ~5 nm. We could optimize the contrast by controlling the etching depth of the grating through adjusting the RIE parameters.

To explain the thermal tuning characteristics of the grating, we express the temperature sensitivity of the resonance wavelength as [7]:

$$\frac{d\lambda_0}{dT} \cong \gamma\Lambda\left(C_{\mathrm{co}} - C_{\mathrm{cl}}\right)\left(\eta_{0\mathrm{co}} - \eta_{m\mathrm{co}}\right) \tag{1}$$

where γ is a modal dispersion factor due to the wavelength dependence of the effective-index difference between the core and cladding modes, C_{co} and C_{cl} are the thermooptic coefficients (TOCs) of the core and cladding materials, respectively, and η_{0co} and η_{mco} are the fractional powers of the core and cladding modes in the core area. As the waveguide parameters γ and ($\eta_{0co} - \eta_{mco}$) change smoothly with the temperature, the sharp change in the temperature sensitivity shown in Fig. 4(a) must be due to a sharp change in the TOCs of the materials.

In a PE $LiNbO_3$ waveguide, the core and the cladding contain different rhombohedral $H_xLi_{1-x}NbO_3$ phases because of their different hydrogen concentrations [14,15]. We can separate the $H_xLi_{1-x}NbO_3$ phases into two groups: the low-index group (e.g., the α phase) and the high-index group (e.g., the β_1 and κ_2 phases) [14,15]. The cladding of our $LiNbO_3$ waveguide went through an annealing process, which results in a lower hydrogen concentration and hence a lower refractive index, and, therefore, should contain more of the first group. On the other hand, the core area went through a second PE and thus contained a higher hydrogen concentration and hence more of the second group. Recently, an experimental study of both z-cut and x-cut PE $LiNbO_3$ waveguides [15] shows that the TOC of the α phase, which has a value of C_1 = 7.0 – 7.6 $\times10^{-5}$ °C^{-1}, remains unchanged in the temperature range 20 – 160 °C, while those of the β_1 and κ_2 phases undergo sharp transitions at temperatures T_C in the range 50 – 60 °C. Below T_C, the TOCs of these phases are C_{2L} = 2.1 – 3.5 $\times10^{-5}$ °C^{-1}, which is smaller than C_1, while above T_C, their value becomes C_{2H} = 12 – 24 $\times10^{-5}$ °C^{-1}, which is larger than C_1 [15]. Therefore, the difference ($C_{co} - C_{cl}$) in Eq. (1) is actually a measure of the difference between the TOCs of the two groups of phases, which should switch from a negative value to a positive value, as the temperature crosses T_C from below, and thus give rise to the results shown in Fig. 4(a). That the transition temperature range in our study (55 – 70 °C) is somewhat different from that reported in Ref. 15 (50 – 60 °C) could be due to the fact that our waveguide contained a more complex phase composition (because of the more complicated fabrication process), whereas the PE waveguide samples used in Ref. 15 contained pure phases. We should note that the microscopic origin of the transition effect is not known for the moment [15]. Our results can be regarded as new experimental evidence of the existence of the effect.

In summary, we demonstrated an LPWG fabricated on a clad $LiNbO_3$ channel waveguide by RIE. The grating had a length of 16 mm and a shallow etching depth of 10 nm, which was capable of generating a rejection band with a contrast up to ~15 dB (at certain temperatures) and a bandwidth of ~5 nm. The grating exhibited a peculiar U-shaped thermal tuning curve – Fig. 4(a), which is attributed to the formation of different $H_xLi_{1-x}NbO_3$ phases in the core and cladding areas of the waveguide [14] and the sharp transitions of the TOCs of certain phases [15]. Regardless of the unusual thermal characteristics, we were able to tune the resonance wavelength of the grating over a range of ~40 nm with a temperature control of ~30 °C. The grating is easy to make and could be further developed into various kinds of $LiNbO_3$-based filters and switches.

The authors wish to thank H. P. Chan and K. P. Lor for useful discussions. This research was supported by a grant from City University of Hong Kong (7008047).

References (OL format)

1. L. Arizmendi, Physica Status Solidi. A, Applied Research **201**, 253 (2004).
2. J. Sochtig, Electron. Lett. **24**, 844 (1988).
3. P. Arora, V. M. Petrov, J. Petter, and T. Tschudi, Opt. Comm. **281**, 2067 (2008).
4. B. E. Benkelfat, R. Ferrière, B. Wacogne, and P. Mollier, IEEE Photon. Technol. Lett. **14**, 1430 (2002).
5. V. Rastogi and K. S. Chiang, Appl. Opt. **41**, 6351 (2002).
6. K. S. Chiang, K. P. Lor, C. K. Chow, H. P. Chan, V. Rastogi, and Y. M. Chu, IEEE Photon. Technol. Lett. **15**, 1094 (2003).
7. Q. Liu, K. S. Chiang, and K. P. Lor, Opt. Lett. **31**, 2716 (2006).
8. W. Jin, K. S. Chiang, Q. Liu, C. K. Chow, H. P. Chan, and K. P. Lor, IEEE Photon. Technol. Lett. **20**, 1258 (2008).
9. W. Jin, K. S. Chiang, and Q. Liu, Opt. Express **20**, 1258 (2008).
10. K. S. Chiang, J. Lightwave Technol. **LT-3**, 385 (1985).
11. K. S. Chiang and S. Y. Cheng, Opt. Eng. **47**, 034601 (2008).
12. P. W. Leech and M. C. Ridgway, J. Vac. Sci. Technol. A **17**, 3358 (1999).
13. M. Tamura and S. Yoshikado, Surf. Coating Tech. **169 –170**, 203 (2003).
14. Y. N. Korkishko and V. A. Fedorov, IEEE J. Select. Topics Quantum Electron. **2**, 187 (1996).
15. A. Alcazarde, B. Ramiro, J. Rams, B. Alonso, G. Rojo, V. Bermudez, and J. M. Cabrera, Appl. Phys. B **79**, 845 (2004).

References (with paper titles)

1. L. Arizmendi, "Photonic applications of lithium niobate crystals," Physica Status Solidi. A, Applied Research, vol. 201, pp. 253-283, 2004.
2. J. Sochtig, "Ti:$LiNbO_3$ stripe waveguide Bragg reflector gratings," Electron. Lett. vol. 24, pp. 844-845, 1988
3. P. Arora, V. M. Petrov, J. Petter, and T. Tschudi, "Integrated optical Bragg filter with fast electrically controllable transfer function," Opt. Comm., vol. 281, 2067-2072, 2008.
4. B. E. Benkelfat, R. Ferrière, B. Wacogne, and P. Mollier, "Technological implementation of Bragg grating reflectors in Ti:$LiNbO_3$ waveguides by proton exchange," IEEE Photon. Technol. Lett., vol. 14, pp. 1430-1432, 2002.
5. V. Rastogi and K. S. Chiang, "Long-period gratings in planar optical waveguides," Appl. Opt., vol. 41, pp. 6351-6355, 2002.
6. K. S. Chiang, K. P. Lor, C. K. Chow, H. P. Chan, V. Rastogi, and Y. M. Chu, "Widely tunable long-period gratings fabricated in polymer-clad ion-exchanged glass waveguides," IEEE Photon. Technol. Lett., vol.15, pp. 1094-1096, 2003.
7. Q. Liu, K. S. Chiang, and K. P. Lor, "Condition for the realization of a temperature-insensitive long-period waveguide grating," Opt. Lett., vol. 31, pp. 2716-2718, 2006.
8. W. Jin, K. S. Chiang, Q. Liu, C. K. Chow, H. P. Chan, and K. P. Lor, "Lithium-niobate channel waveguide for the realization of long-period gratings," IEEE Photon. Technol. Lett., vol. 20, pp. 1258-1260, 2008.
9. W. Jin, K. S. Chiang, and Q. Liu, "Electro-optic long-period grating in lithium-niobate waveguide," Opt. Express, vol. 20, pp. 1258-1260, 2008.

10. K. S. Chiang, “Construction of refractive-index profiles of planar dielectric waveguides from the distribution of effective indexes,” J. Lightwave Technol., vol. LT-3, pp. 385-391, 1985.

11. K. S. Chiang and S. Y. Cheng, “A technique of applying the prism-coupler method for accurate measurement of the effective indices of channel waveguides,” Opt. Eng., vol. 47, 034601(1-4), 2008.

12. P. W. Leech and M. C. Ridgway, “Enhancement of the etch rate of $LiNbO_3$ by prior bombardment with MeV O^{2+} ions,” J. Vac. Sci. Technol. A, vol. 17, pp. 3358-3361, 1999.

13. M. Tamura and S. Yoshikado, “Etching characteristics of $LiNbO_3$ crystal by fluorine gas plasma reactive ion etching,” Surf. Coating Tech., vol. 169 –170, pp. 203–207, 2003.

14. Y. N. Korkishko and V. A. Fedorov, “Structural phase diagram of $H_xLi_{1-x}NbO_3$ waveguides: the correlation between structural and optical properties,” IEEE J. Select. Topics Quantum Electron., vol. 2, pp. 187-196, 1996.

15. A. Alcazarde, B. Ramiro, J. Rams, B. Alonso, G. Rojo, V. Bermudez, and J. M. Cabrera, “Temperature effects in proton exchanged $LiNbO_3$ waveguides,” Appl. Phys. B, vol. 79, pp. 845-849, 2004.

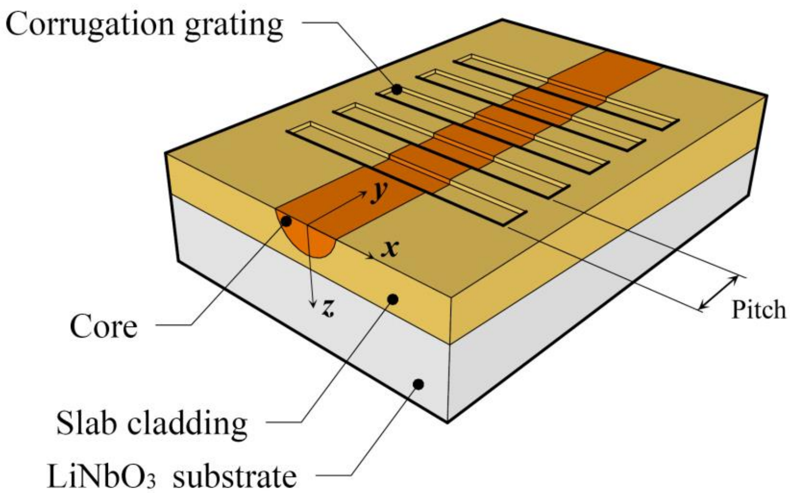

Fig. 1. Schematic diagram of a long-period corrugation grating formed on a clad $LiNbO_3$ channel waveguide.

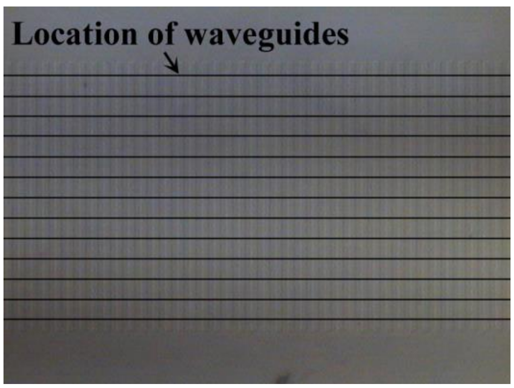

(a)

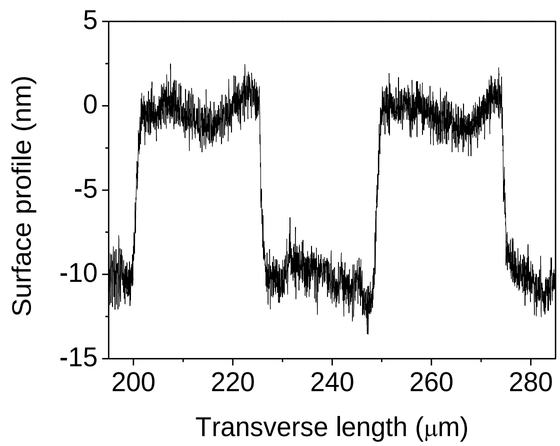

(b)

Fig. 2. (a) Optical image and (b) surface profile of the fabricated corrugation grating.

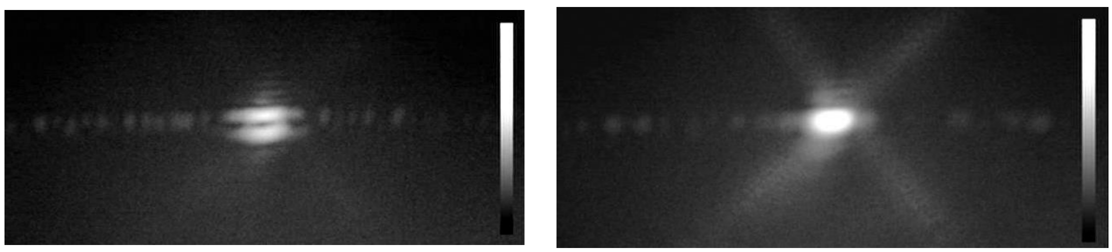

(a) (b)

Fig. 3. Near-field images taken from the output of the grating at 25 ^{o}C: (a) at the resonance wavelength 1584 nm and (b) at the off-resonance wavelength 1560 nm.

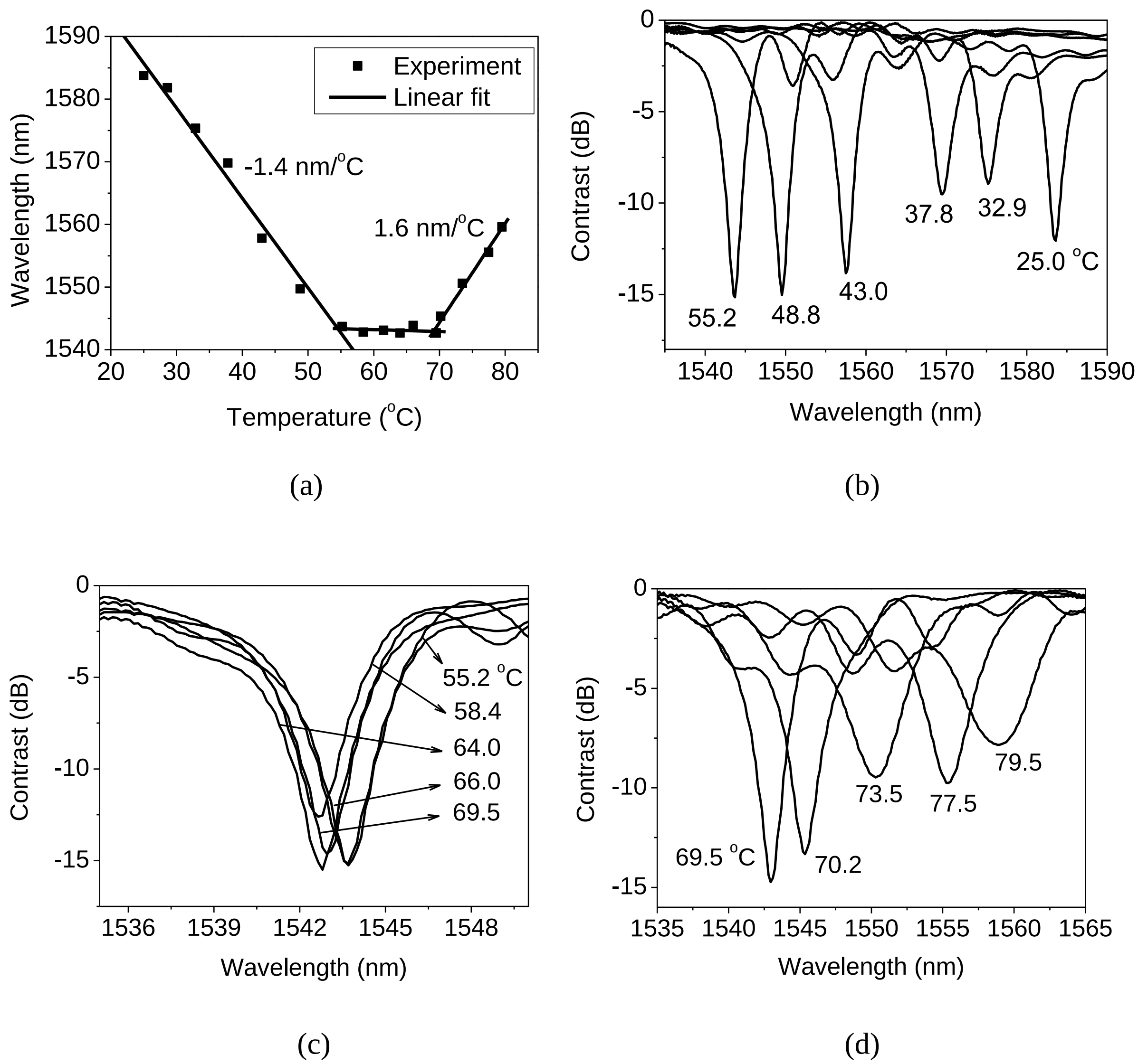

Fig. 4. (a) Change of the resonance wavelength of the grating with the temperature, and (b) normalized transmission spectra measured from 25 to 55.2 ^{o}C; (c) from 55.2 to 69.5 ^{o}C; and (d) from 69.5 to 79.5 ^{o}C.